

# Anomalous diffusion dynamics of learning in deep neural networks

Guozhang Chen,<sup>1</sup> Cheng Kevin Qu,<sup>1</sup> and Pulin Gong<sup>1,\*</sup>

<sup>1</sup>*School of Physics, University of Sydney, Sydney, NSW 2006, Australia*

(Dated: November 15, 2021)

Learning in deep neural networks (DNNs) is implemented through minimizing a highly non-convex loss function, typically by a stochastic gradient descent (SGD) method. This learning process can effectively find good wide minima without being trapped in poor local ones. We present a novel account of how such effective deep learning emerges through the interactions of the SGD and the geometrical structure of the loss landscape. Rather than being a normal diffusion process (i.e. Brownian motion) as often assumed, we find that the SGD exhibits rich, complex dynamics when navigating through the loss landscape; initially, the SGD exhibits anomalous superdiffusion, which attenuates gradually and changes to subdiffusion at long times when the solution is reached. Such learning dynamics happen ubiquitously in different DNNs such as ResNet and VGG-like networks and are insensitive to batch size and learning rate. The anomalous superdiffusion process during the initial learning phase indicates that the motion of SGD along the loss landscape possesses intermittent, big jumps; this non-equilibrium property enables the SGD to escape from sharp local minima. By adapting the methods developed for studying energy landscapes in complex physical systems, we find that such superdiffusive learning dynamics are due to the interactions of the SGD and the fractal-like structure of the loss landscape. We further develop a simple model to demonstrate the mechanistic role of the fractal loss landscape in enabling the SGD to effectively find global minima. Our results thus reveal the effectiveness of deep learning from a novel perspective and have implications for designing efficient deep neural networks.

## I. INTRODUCTION

Deep neural networks (DNNs) trained by stochastic gradient descent (SGD) have achieved great success in many application areas [1]. As often assumed, the SGD optimizer of highly non-convex loss functions is rarely trapped in local minima, and effectively finds wide ones with good generalization [2, 3]. Understanding how this property emerges from the DNNs is of fundamental importance for deciphering the secret of the remarkable effectiveness of deep learning [4].

Recently, progress has been made in either characterizing the structure of loss functions or the dynamics of SGD for gaining comprehension of deep learning. For instance, the characterizations of loss functions have been studied by using random matrix theory [5], algebraic geometry methods [6] and some visualization-based methods [7]. The dynamics of SGD have been extensively studied via models of stochastic gradient Langevin dynamics with an assumption that gradient noise is Gaussian [8, 9]; in these models, the SGD is driven by Brownian motion in particular. However, it has been increasingly realized that such Brownian motion-based characterizations of SGD dynamics are inappropriate, as SGD dynamics commonly exhibit highly anisotropic and dynamic-changing properties [10–13], suggesting the presence of rich, complex learning dynamics in DNNs. Despite the progress made by these studies, the fundamental questions of how the interaction of SGD with the structure of the loss function gives rise to complex learning dynamics, and whether and

how such dynamics enable SGD to find wide minima remain unresolved.

In this study, by adapting the methods developed in nonequilibrium physical systems, we find that the interactions of the fractal loss landscape and the SGD give rise to complex learning dynamics; these include anomalous superdiffusion during the initial learning phase, which changes to subdiffusion at long times when a solution is reached. The fractal-like structure of loss landscape indicates that it possesses varying steepness (Fig. 1) and that the corresponding loss gradient displays large fluctuations with heavy-tailed distributions, thus resulting in superdiffusive learning dynamics. Superdiffusion consists of small movements that are intermittently interrupted by big jumps, which enable the SGD to escape from local minima; this computational advantage of superdiffusion is further illustrated in a simple model where the SGD interacts with a low-dimensional fractal loss landscape.

## II. DNNs SETUP AND CHARACTERIZATIONS OF ANOMALOUS DIFFUSION DYNAMICS

### A. DNNs setup

We consider two classes of neural networks: 1) ResNet-14/20/56/110 [14], where each type is labeled with the number of layers it has. 2) VGG-like networks that do not contain shortcut/skip connections. We produce these networks simply by removing the shortcut connections from ResNets, termed ResNet-14/20/56/110-noshort. All models are trained by vanilla SGD on multiple datasets including MNIST and CIFAR-10, by using two loss functions (i.e., cross-entropy, and mean-square-

---

\* pulin.gong@sydney.edu.au

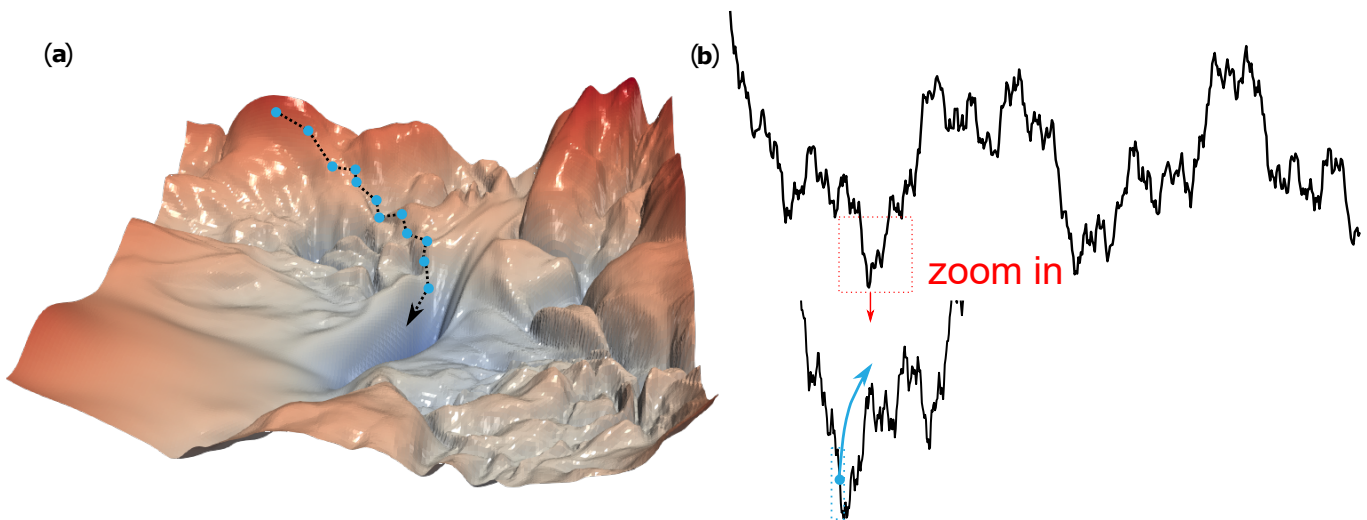


FIG. 1. **Schematic diagram of non-convex loss landscape with a fractal-like structure.** (a) The log-value of loss landscape is projected to 2D. The training process based on SGD can be regarded as a SGD optimizer moving on the loss landscape. (b) The fine structure of non-convex loss landscape with a fractal structure shows self-similar and hierarchical properties.

error losses). The training processes each run for 500 epochs. All networks are initialized in the standard procedures of the PyTorch library (version 1.3.0). Source code is available at <https://github.com/ifgovh/Anomalous-diffusion-dynamics-of-SGD.git>.

### B. Characterizations of anomalous diffusion learning dynamics

Given that full-batch gradient descent is computationally expensive, in the SGD algorithm, the weight parameters  $\mathbf{w} = (w_1, w_2, \dots, w_d)$  are estimated by minimizing the minibatch loss function  $\nabla \tilde{L}(\mathbf{w}) : \mathbb{R}^d \rightarrow \mathbb{R}$ , according to

$$\mathbf{w}_{t+1} = \mathbf{w}_t - \eta \nabla \tilde{L}_t(\mathbf{w}_t), \quad (1)$$

where  $\mathbf{w}_t$  denotes the  $d$ -dimension weight vector  $(w_1, w_2, \dots, w_d)$  at time  $t$ , and  $\eta$  corresponds to the learning rate. The absence of the partial dataset generates gradient noise  $U_t \triangleq \nabla \tilde{L}_t(\mathbf{w}_t) - \nabla L_t(\mathbf{w}_t)$ . The updating rule can be rewritten as:

$$\mathbf{w}_{t+1} = \mathbf{w}_t - \eta \nabla L_t(\mathbf{w}_t) + U_t, \quad (2)$$

Hence the SGD training process can be regarded as a random diffusive process, where  $\mathbf{w}$  can be geometrically interpreted as coordinates of the SGD optimizer in the loss landscape  $L$  (Fig. 1).

The loss function of DNN exhibits complex structures, as demonstrated by the projected 2D loss landscape of ResNet-56-noshort [7] (Fig. 1), analogous to complex energy landscape in physical systems [15–18]. In these physical systems, energy landscapes possess fractal-like structures and anomalous diffusion motions of particles

stem directly from such fractal structures. In this study, we apply similar methods used in these systems to quantify the diffusion dynamics of the SGD optimizer. Particularly, the time-average mean squared displacement (MSD) is used to characterize the dynamics of SGD moving through the loss landscape, which is defined as

$$\Delta r^2(t_w, \tau) = \frac{1}{T} \sum_{t=t_w}^{t_w+T} \sum_{i=1}^d (w_i(t+\tau) - w_i(t))^2, \quad (3)$$

where  $\tau$  is lag time,  $T$  is the length of the time interval  $[t_w, t_w + T]$ , and  $w_i(t)$  is the value of the  $i^{\text{th}}$  weight at time  $t$ .

Brownian motion is characterized by  $\Delta r^2(\tau) \propto \tau^\alpha$ , with  $\alpha = 1$ ; the MSD is a linear function of lag time  $\tau$ . When the diffusion exponent  $\alpha \neq 1$ , the corresponding diffusion process has a nonlinear relationship with respect to  $\tau$  and is defined as anomalous diffusion [19]. If  $1 < \alpha < 2$ , it is a superdiffusive process; superdiffusion consists of small movements that are intermittently interrupted by long-range jumps. This process has been widely observed in complex physical systems and biological systems [20]; the mixture of small movements and big jumps in this process is essential for optimally transporting energy in turbulent fluid [21], and for animals to optimally search for spatially distributed food [22]. If  $0 < \alpha < 1$ , the optimizer is subdiffusive and mainly explores local areas.

## III. RESULTS

### A. Anomalous diffusion of SGD dynamics

We first illustrate that the anomalous diffusion process characterizes SGD learning dynamics. As the findings of

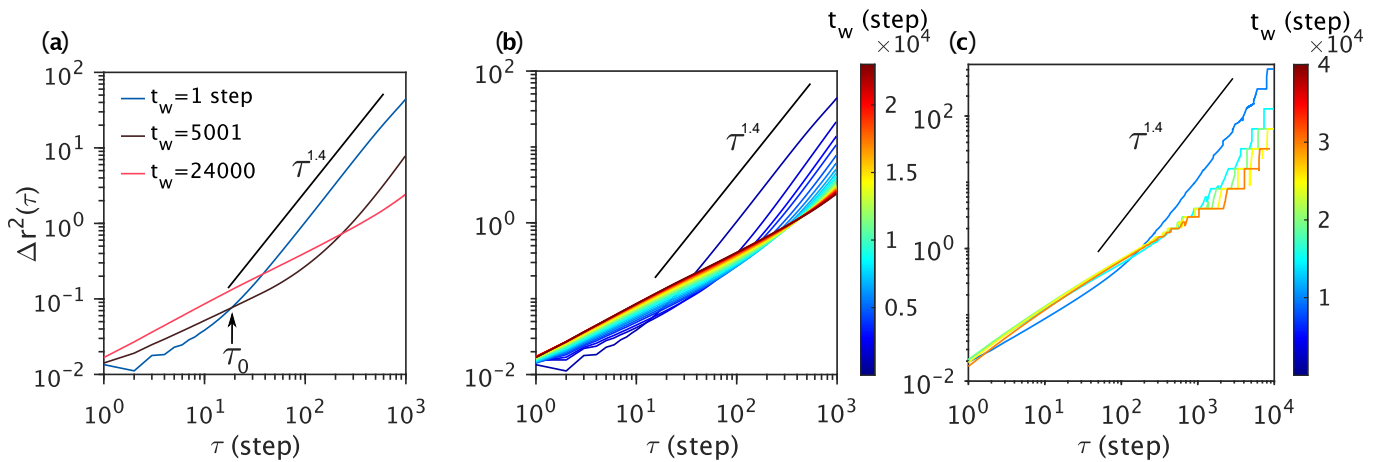


FIG. 2. **SGD dynamics are anomalous diffusion.** (a) MSD  $\Delta r^2(\tau)$  of SGD as a function of lag time  $\tau$  in interval  $[t_w, t_w + T]$ ,  $T = 1000$ . (b) Same as in (a) but the starting time of the interval  $t_w$  gradually increases from 1 to 24000 steps, covering the whole training process. (c) Same as in (b) but for  $T = 10000$ .

different DNN settings are similar, we thus demonstrate all results in ResNet-14 with a batch size of 1024, trained on CIFAR-10 with the cross-entropy loss function and a learning rate of 0.1, unless stated otherwise.

The MSD of each interval  $[t_w, t_w + T]$  is calculated according to Eq. 3 ( $T = 1000$ ) for a given  $t_w$ . To demonstrate how the diffusion dynamics of SGD optimizer change during the training process, we change  $t_w$  accordingly. As shown in Fig. 2(a), there are two regimes of the learning dynamics characterized by the diffusion exponent  $\alpha$ . For the first regime  $t_w < t_0$ ,  $t_0 = 21000$  (blue curve, Fig. 2(a)), MSD curves have two segments on the scale  $\tau \in [1, T]$  with the smooth transitions around  $\tau_0$  ( $\tau_0$  is labeled in Fig. 2(a)). When the lag time  $\tau > \tau_0$  ( $\tau_0$  is labeled in Fig. 2(a)), MSD curve can be fitted to  $\Delta r^2(\tau) \propto \tau^\alpha$  with  $\alpha > 1$ , indicating that the SGD optimizer is superdiffusive. However, when  $\tau < \tau_0$ ,  $\alpha < 1$ , i.e. the SGD dynamics are subdiffusive (Fig. 2(a)). During the initial phase of the training process, the interval of the superdiffusion is much longer than that of the subdiffusion. Nevertheless, as  $t_w$  increases, the superdiffusion gradually attenuates, as demonstrated by the decrease of the diffusion exponent  $\alpha$  and the increase of  $\tau_0$  (brown curve in Fig. 2(a); all curves are shown in Fig. 2(b)). In the second regime  $t_w > t_0$ , the diffusion exponent  $\alpha = 0.78$ , i.e., the subdiffusion process eventually emerges, as shown by the red curve in Fig. 2(a). Note that the interval  $T$  does not affect the transition phenomenon as shown in Fig. 2(c). These changes in the anomalous diffusion during the training process indicate that the SGD learning dynamics are different from the Brownian motion and exhibit rich, non-equilibrium dynamics.

Such anomalous diffusion dynamics provide a way to characterize contributions of network structures and different hyperparameters to the training process. We train two types of DNNs, i.e., ResNet and VGG-like networks. VGG-like networks are produced simply by removing the

shortcut connections from ResNets. As shown in Fig. 3, shortcut connections do not change the diffusion exponent  $\alpha$  significantly in both regimes; however, they do affect the scale range of superdiffusion characterized by  $\tau_0$ . Specifically, with shortcut connections,  $\tau_0$  is smaller than those without shortcut connections, indicating that the scale of superdiffusion is elongated (Fig. 3(b) and Fig. 3(d)). As superdiffusion can explore larger areas in a fixed time than subdiffusion, DNNs with shortcut connections facilitate training, which is consistent with previous studies [7, 14].

The anomalous diffusion learning dynamics are not very sensitive to minibatch sizes. As shown in Fig. 3(a), the diffusion exponent  $\alpha$  in the first regime does not significantly vary ( $\pm 15\%$ ) with respect to the change of minibatch size from 128 to 1024 in all networks, although  $\tau_0$  decreases in ResNet-14,20 with the increase of minibatch size (Fig. 3(b)).

Furthermore, as shown in Fig. 3(c),  $\alpha$  changes nonlinearly with respect to the network depth. However, the network depth reduces the scale range of superdiffusion, characterized by  $\tau_0$  (Fig. 3(d)). These results suggest that the deeper DNNs are more difficult to be trained due to the shorter scale of superdiffusion.

We next demonstrate that varying learning rates from 0.001 to 0.5 only influence the emerging sequence of the superdiffusion learning dynamics (Fig. 4(a)). As shown in Fig. 4(b), DNN training with small learning rates are much slower than that with large learning rates; thus, the training progress with small learning rates is delayed, compared with large learning rates. Thus, a small or large learning rate can only slow down or speed up the training procedure, but does not change the fundamental occurrence of anomalous diffusion dynamics as the learning rate is merely a discretized realization of SGD. When the learning rate is small ( $\eta < 0.05$ ), during 500 epochs, the training processes remain in the first regime; there is no pure subdiffusion in Fig. 4(c) and Fig. 4(d). For

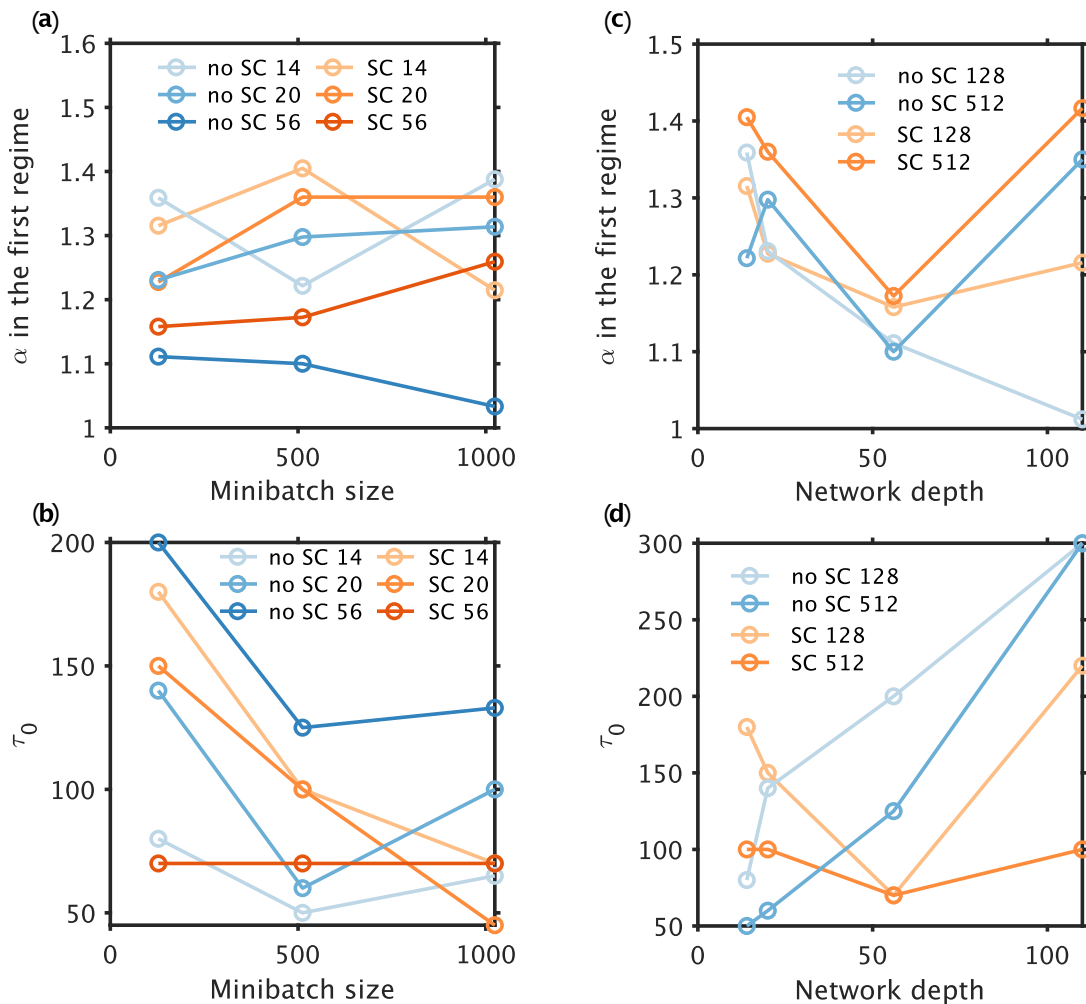


FIG. 3. **The effects of the depth, batch size, and shortcut connections of DNNs on the anomalous diffusion dynamics of SGD.** The orange and blue colors represent the network with/without shortcut connections (SC) respectively. The digits in legends of **a-b** represent network depth; for example, no SC 14 denotes the ResNet-14-noshort. Those in **c-d** represent minibatch size; for example, no SC 128 denotes ResNet training using the minibatch size of 128. (a) The diffusion exponents  $\alpha$  on larger lag times ( $\tau > \tau_0$ ) when  $t_w = 1$  as a function of minibatch size. (b) The crossover  $\tau_0$  as a function of minibatch size.  $\tau_0$  is the lag time when the MSD curve transitions from subdiffusion to superdiffusion when  $t_w = 1$ . (c) Similar to (a) but for varying network depth. (d) Similar to (b) but for varying network depth.

example, when  $\eta = 0.001$ , the MSD curves for  $t_w < 5000$  have only one segment instead of two and a diffusion exponent of  $\alpha = 2$ . This is due to the SGD optimizer taking steps on small learning rates which require a long time to enter narrow minima, resulting in the optimizer moving toward one direction (ballistic limit,  $\alpha = 2$ ). However, DNNs trained with larger learning rates grant superdiffusion in the first regime and pure subdiffusion dynamics in the second regime, as shown in Fig. 4(e) and Fig. 4(f).

### B. Heavy-tailed gradients

We next demonstrate the statistical property of minibatch gradients  $\nabla\tilde{L}$ . We calculate  $\nabla\tilde{L}$  by vanilla SGD with respect to each  $w_i$  at each time point, and find that

$\nabla\tilde{L}$  in the first regime ( $t_w < t_0$ ,  $t_0 = 21000$ ) can be fitted to a symmetric Lévy stable distribution (stability parameter  $\alpha_{\text{dist}} = 1.47$  [1.46509, 1.46546]; the brackets denote the 95% confidence interval calculated by the maximum likelihood method; Fig. 5(a)). Given a symmetric Lévy stable random variable  $X$ , its probability density function (PDF) decays with a power-law tail  $|x|^{-\alpha_{\text{dist}}-1}$  which is much slower compared to Gaussian distributions, thus they have heavy tails [23]. The power-law tail of the distribution of  $\nabla\tilde{L}$  shown in Fig. 5(a) inset further validates the heavy-tailed distribution. We further compare log-likelihood ratios between the fitted stable distribution and Gaussian distribution, and find that the log-likelihood ratios ( $1.52 \times 10^9$ ) are sufficiently positive, indicating that the distributions most likely follow Lévy stable distribution ( $p < 10^{-15}$ , Vuong test).

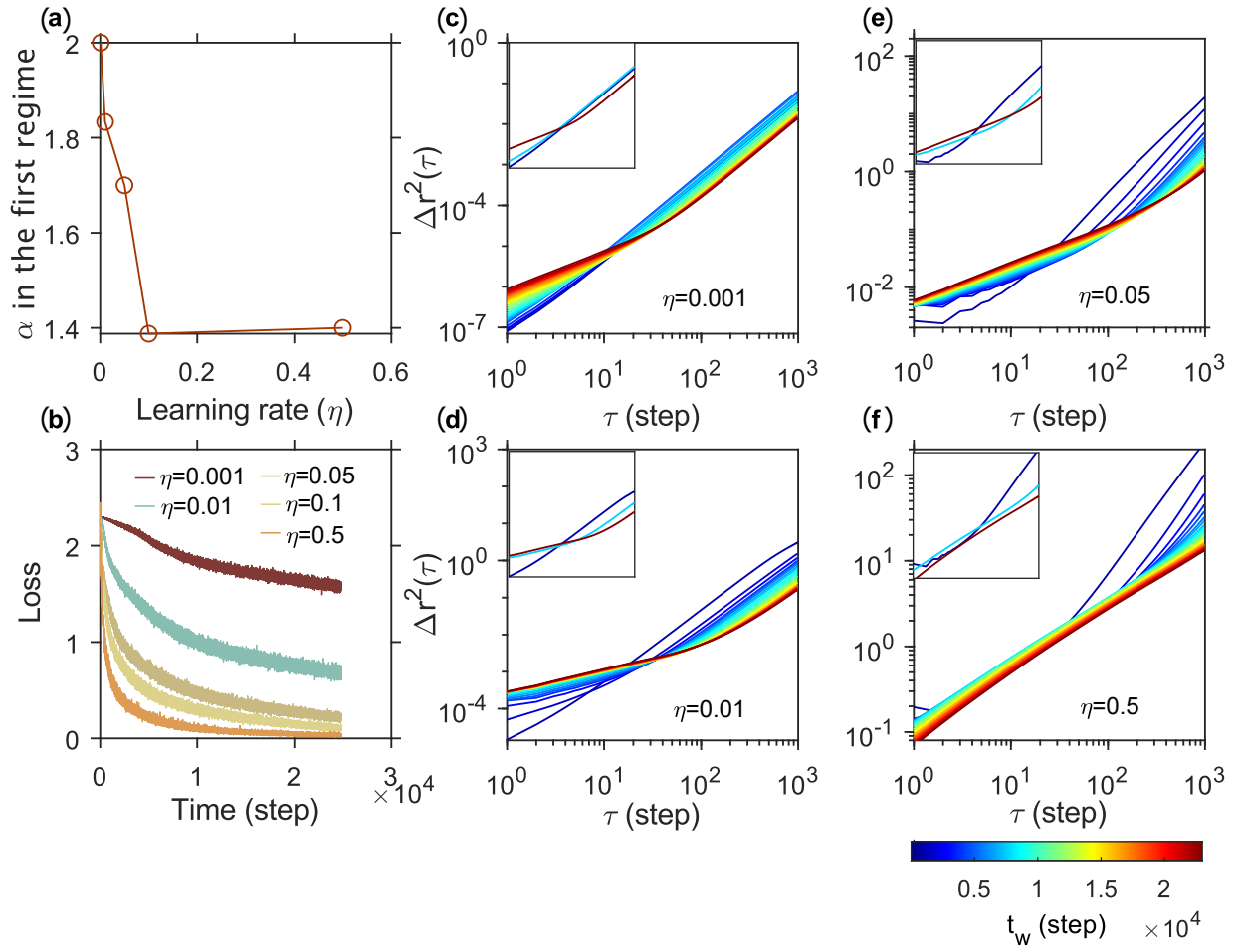


FIG. 4. **The effect of learning rate on the anomalous diffusion dynamics of SGD.** All results are from ResNet-14 with a batch size of 1024 on CIFAR10 dataset. (a) The diffusion exponent  $\alpha$  on larger lag times ( $\tau > \tau_0$ ) when  $t_w = 1$  as a function of learning rate  $\eta$ . (b) The loss value as a function of time. **c-f** The MSD of SGD for the learning rates of 0.001, 0.01, 0.05, and 0.5, respectively. Jet colormap represents the starting time point ( $t_w$ ) as in Fig. 2(b). One curve represents MSD in 1000 steps. Inset: The MSD of SGD when  $t_w = 1, 7001, 23001$ .

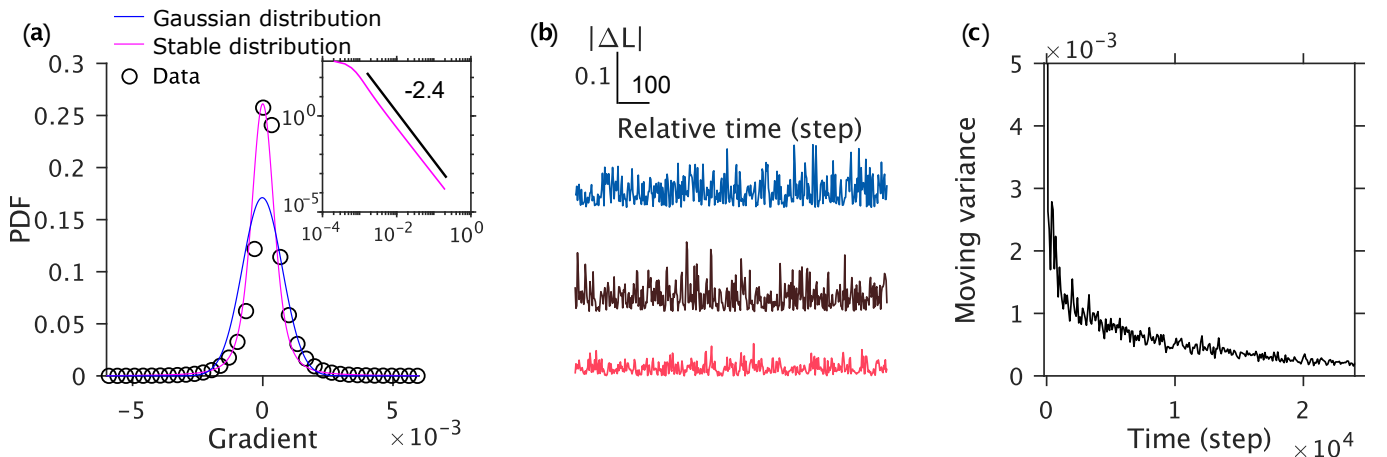


FIG. 5. **The gradient is heavy-tailed.** The distribution of minibatch gradients  $\nabla \tilde{L}(\mathbf{w})$  in the first regime can be fitted as a symmetric Lévy stable distribution (red curve). Inset: the log-log plot of the positive part of the distribution indicates that it has a power-law tail. (b) Fluctuations of absolute value of change-of-loss  $\Delta L$  decrease as  $t_w$  increases. Colormap is the same as in Fig. 2(a). (c) The moving variance of loss as a function of time.

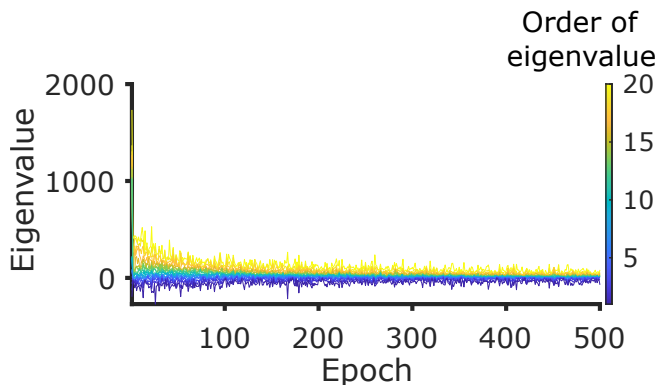


FIG. 6. **The top 20 eigenvalues of Hessian matrix of loss landscape decrease as training epoch increases.** This indicates that the SGD optimizer leaves narrow local minima and enters a flatter area in the loss landscape of DNN.

The heavy-tailed gradient  $\nabla \tilde{L}$ , according to Eq. 1, gives rise to long-range jumps ( $\mathbf{w}_{t+1} - \mathbf{w}_t$ ) that result in superdiffusion processes. These long-range jumps caused by heavy-tailed gradients can help the optimizer jump out narrow minima, causing the large fluctuation of loss values ( $L$ ). To demonstrate the fluctuations, we first calculate the absolute value of change-of-loss  $|\Delta L| = L(\mathbf{w}(t+1) - \mathbf{w}(t))$ . As shown in Fig. 5(b), as  $t_w$  increases,  $|\Delta L|$  decreases. Such behavior is further quantified by the decreasing moving variance of the loss  $L$  against time (Fig. 5(c)); the moving variance is calculated over a sliding window of 100 steps across neighboring  $L$ .

A local optimum that generalizes well is generically expected within a flat basin where the loss changes by very little or not at all (we will use flat colloquially to indicate approximate flatness) rather than being a narrow minimum [24, 25]. Thus, SGD aims to leave the narrow minima and enter one with the most amount of flat directions, which is also quantified by that eigenvalues of the Hessian matrix gradually decrease to near zero values (Fig. 6). Directions along Hessian eigenvectors with negative eigenvalues have curvature downward. Directions with positive eigenvalues have upward curvature. Zero eigenvalues represent flat directions[25]. This preference for flat minima can be explained by the anomalous diffusion dynamics. In the first regime ( $t_w < t_0$ ), the narrow, rough, and non-convex loss landscape of DNN can provide sufficiently large gradients ( $\nabla \tilde{L}$ , Fig. 1(b)) allowing for long-range jumps. Thus, superdiffusion emerges and the SGD optimizer escapes narrow minima. In contrast, flatter minima in the second regime cannot provide large minibatch gradients as characterized by the reduced stability parameter (1.61) of gradients in the second regime. Therefore, due to increasingly flat directions, superdiffusion attenuates and instead subdiffusion occurs in the second regime ( $t_w > t_0$ ). Thus, the anomalous diffusion dynamics result from the interaction of SGD and geometrical structures of loss landscape.

### C. Fractal-like loss landscape

In physical systems, complex energy landscapes often exhibit fractal structures with self-similar and hierarchical properties [15, 16, 18] and such structures can cause anomalous diffusion motions of particles [16]. We now demonstrate that the loss landscapes of DNNs also have fractal-like structures. From [26], the definition of fractal is as the following:

**Definition** A random function  $L$  on a metric space is fractal if the distribution of  $L(X')$  conditional on  $L(X)$ ,  $X$ , and  $X'$ , is normal with mean 0 and variance proportional to  $\Delta r(X', X)^{2H}$ , where  $H$  is a parameter in  $(0, 1)$  and  $\Delta r(X', X)$  is the distance between point  $X$  and  $X'$ .

The distribution in the definition is sampled over random values of  $X$  and  $X'$  for a given sample function  $L$ , experimentally. The equivalence of these two procedures is referred to as ergodicity. Checking the distributions of each value of distance in practice is difficult; hence we measure the expectation of  $[L(X') - L(X)]^2$  (i.e., mean squared loss differences of pairs, MSL) to characterize the fractal-like structure if MSL satisfies the following relation. Note that in the field of machine learning, the same method has been used to quantify fractal landscapes for simulated annealing [27].

$$\text{MSL} \propto \Delta r(\mathbf{w}, \tilde{\mathbf{w}})^{2H}, \quad (4)$$

where  $\Delta r(\mathbf{w}, \tilde{\mathbf{w}})^{2H}$  is the end-to-end distance between  $\mathbf{w}$  and  $\tilde{\mathbf{w}}$ .

The MSL is calculated by the following equation,

$$\text{MSL}(t_w, \Delta r) = \frac{1}{C_{\Delta r}} \sum_{j=1}^{C_{\Delta r}} L(\mathbf{w}_{\Delta r}^{t_w, T}(j)) - L(\tilde{\mathbf{w}}_{\Delta r}^{t_w, T}(j)), \quad (5)$$

where the weights  $\mathbf{w}_{\Delta r}^{t_w, T}(j)$  and  $\tilde{\mathbf{w}}_{\Delta r}^{t_w, T}(j)$  are a pair of weights at different time steps in  $[t_w, t_w + T]$  and the end-to-end distance between this pair is  $\Delta r$ , and  $C_{\Delta r}$  is the number of pairs at a distance of  $\Delta r$ . To be consistent with piecewise MSD, we choose  $T = 1000$  steps. We use the points sampled by SGD (i.e., points along the optimization trajectory) to estimate MSL; it sheds light on the local area of the loss landscape that we would like to explore.

As shown in Fig. 7(a) (red curve), in the first regime ( $t_w < t_0$ ), the MSL curve can be fitted to a power-law function with an exponent of 1.8 on the larger distance scale ( $\Delta r \in [0.4, 10]$ ). It satisfies Eq. 4 and indicates that the loss landscape of DNN has fractal-like structures at the initial phase of learning process, analogous to the fractal landscape of simulated annealing [27]. Note that the power-law scalings do not hold within the whole scale ( $[0.1, 10]$ ), which is reasonable because the loss function is differentiable everywhere whilst a full-scale fractal is not. The scaling of the landscape satisfies the differentiability requirement and maintains fractal-like hierarchical

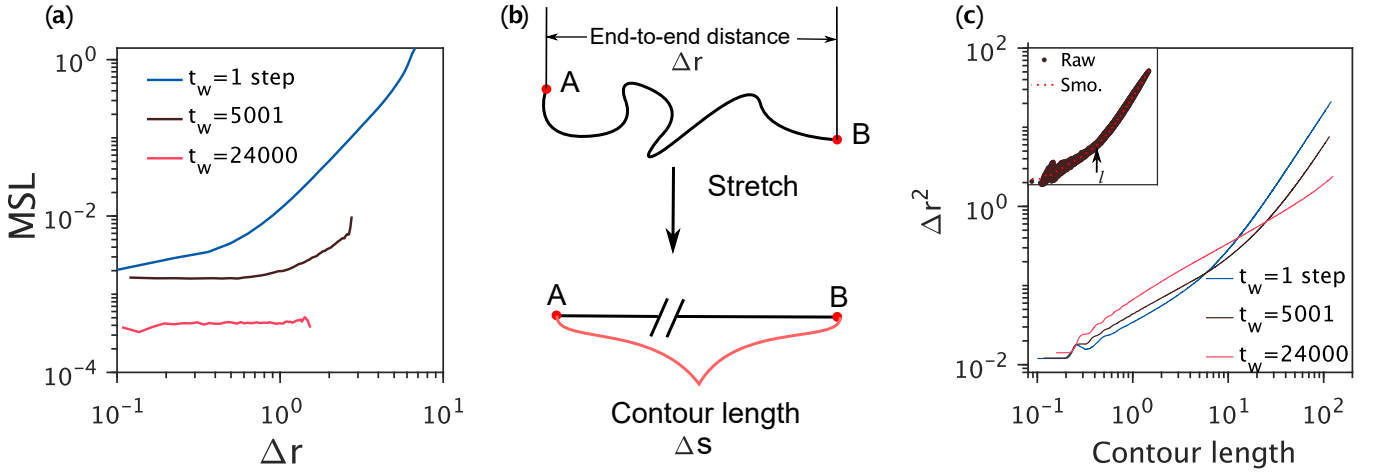


FIG. 7. **The fractal loss landscape of DNN and SGD path.** (a) Mean squared loss differences of point pairs (MSL) against the end-to-end distances  $\Delta r$  in the interval  $[t_w, t_w + T]$ . (b) Schematic diagram of contour length  $\Delta s$  and end-to-end distance  $\Delta r$ . (c) Squared end-to-end displacement ( $\Delta r^2$ ) as a function of contour length. The colormap is the same as in (a). The curve is smoothed by moving average over each window of raw data for clearer illustration; the window length is 40 steps. The inset displays the raw data when  $t_w = 1$  and the dashed red line represents the smoothed data.

structures on larger scales. As the superdiffusion attenuates, the end-to-end distance  $\Delta r$  in  $T$  decreases and the power-law exponent of the MSL with respect to  $\Delta r$  flattens from period to period (brown curve in Fig. 7(a)). Eventually, in the second regime ( $t_w > t_0$ ), the MSL is around a constant value against varying  $\Delta r$  (red curve in Fig. 7(a)). Importantly, these time-inhomogeneous behaviors are consistent with the anomalous diffusion of SGD. When  $t_w < t_0$ , the fractal-like hierarchical structure may provide heavy-tail gradients and thus superdiffusion emerges; when  $t_w > t_0$ , the MSL converges to constant, potentially because the optimizer enters a flat basin eventually.

To further demonstrate the fractal-like structure of loss landscape, we use the method of filter-wise normalized directions [7] to project the loss landscape of ResNet-14 with the batch size of 1024 to 2D space. We then calculate the Hausdorff dimension of a 2D projected loss landscape via the box-counting method, and the fractal dimension is approximately 1.8.

#### D. Fractal trajectory of SGD

Because of the fractal structures of loss landscapes, the paths taken by SGD are expected to be fractal as found in complex energy landscapes [16]. To verify that the SGD path is indeed fractal, we characterize the power-law scaling of end-to-end length and contour length as used in [16]. Specifically, the contour length is the path length from one end to another and is calculated by accumulating step sizes as illustrated in Fig. 7(b). As shown in Fig. 7(c), the segmented end-to-end distance ( $\Delta r$ ) of SGD path appears to scale with its contour length,  $\Delta s$ . The data is smoothed to be clear; the example of raw

data and the smoothed data are shown in Fig. 7(c) inset. The blue and brown curves in Fig. 7(c) display two distinct scaling regimes, illustrating the self-similarity of SGD paths in certain ranges [16]. The fractal dimension  $D_f$  is calculated by the scaling of  $\Delta s$  and  $\Delta r$  ( $\Delta r^2 \sim \Delta s^\lambda$ ),  $D_f = (2/\lambda) \in [1.32, 2.67]$ . Separated by the crossover  $l$  (labeled in Fig. 7(c) inset),  $\lambda$  on longer length scales ( $\Delta s > l$ ) is larger than that on short length scales ( $\Delta s < l$ ). As  $t_w$  increases, MSL collapse to a power law with an exponent of 0.75 (red curve in Fig. 7(c)). The time-inhomogeneous dynamical changes of SGD trajectory are similar to the case of the MSD (Fig. 2(a)) and MSL (Fig. 7(a)).

#### E. Fractal-like landscapes can cause anomalous diffusion learning dynamics

To further understand the contributions of fractal-like loss landscapes to the anomalous diffusion of learning dynamics, we develop a simplified model of SGD with a 2D fractal loss landscape, as described below.

$$\mathbf{w}_{t+1} = \mathbf{w}_t - \eta \nabla L(\mathbf{w}_t) + \eta \sigma Z_t, \quad (6)$$

where  $\mathbf{w}_t$  is the weight parameters at time  $t$ ,  $\eta$  is the learning rate, and  $Z_t$  is drawn from Gaussian distribution  $\mathcal{N}(\mathbf{0}, \sigma)$ . The landscapes of  $L$  are fractal on a 2D space and are generated by the algorithm in [28] with fractal dimension  $\in [1, 2]$  (Fig. 8(a)). Among the generated landscapes, those which contain a wide minimum are selected, simulating the flat basin (local optima) in loss landscapes of DNNs. In such landscapes, we iterate Eq. 6 1000 times with the learning rate  $\eta \in [0.002, 0.01]$  and  $\sigma \in [0.005, 0.05]$ , and the gradient  $\nabla L$  is calculated by the numerical gradient of the landscape. The SGD

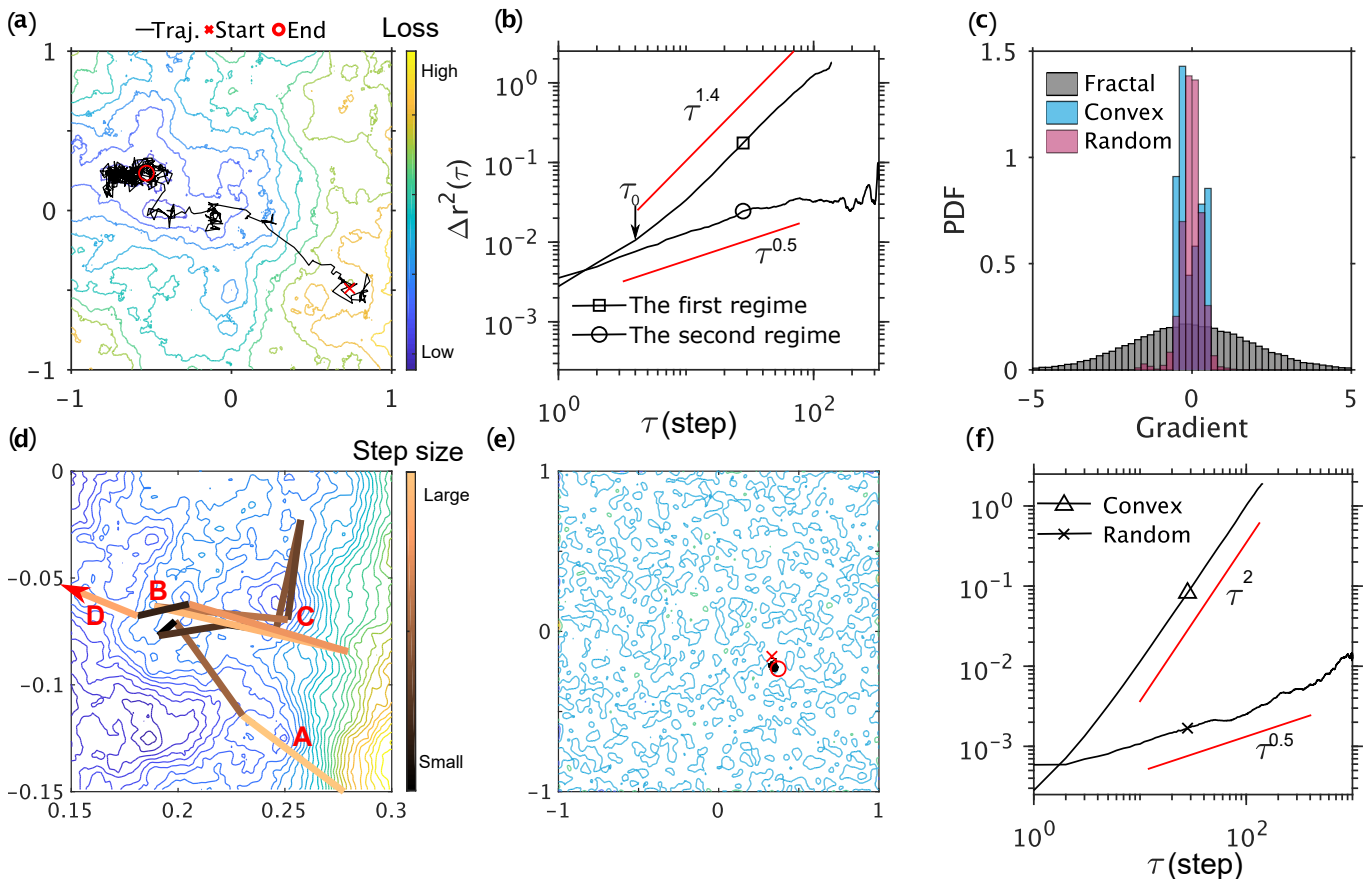


FIG. 8. **The simplified model unravels the anomalous diffusion nature of the SGD optimizer.** (a) Black curve represents the trajectory of the SGD optimizer in the simplified model on the 2D fractal loss landscape illustrated by the contour plot. (b) MSD of the SGD optimizers in the fractal landscape as the function of lag time. (c) Distributions of gradients ( $\Delta L$ ) in fractal, convex, and randomly shuffled landscapes, respectively. (d) Trajectory of the SGD optimizer and the landscape in (a) are zoomed in around a local minimum. The colormap from black to golden encodes the step sizes. (e) Same as in (a) but for random landscape. (f) Same as in (b) but for random landscape and convex landscape.

optimizer moves from a high-altitude point to the global minimum, as the example ( $\eta = 0.02$  and  $\sigma = 0.01$ ) shown in Fig. 8(a). The MSD also illustrates that the SGD optimizer is dominantly superdiffusive when  $t_w < t_0 = 139$  (before entering the final minimum; curve with a square in Fig. 8(b)). When  $t_w > t_0$  (after entering the final minimum), the dynamics of SGD optimizer are only subdiffusive as shown in the curve with a circle in Fig. 8(b). Such behaviors demonstrate that the simple model can reproduce the time-inhomogeneous MSD of SGD as found in DNNs.

In this model with 2D fractal landscape, the fractal landscape generates a heavy-tailed distribution of gradients ( $\nabla L$ ) of all steps (Fig. 8(c)). As found in the DNNs, the gradient distribution can be fitted as a symmetric Lévy stable distribution which has the stability parameter  $\alpha_{\text{dist}} = 1.9$  [1.88749, 1.91298]. The goodness of fit is verified by the positive log-likelihood ratio (39.37) of stable distribution and normal distribution. In our model,  $\nabla L$  is calculated by the numerical gradient of the fractal landscape when  $t_w < t_0$ . Such heavy-tailed gradi-

ents provide a relatively higher possibility of long-range jumps, which generate superdiffusion. In the fine structure of fractal landscape, there are large gradient values (Fig. 1(b)) which propel the SGD optimizer to jump out narrow minima. It is important to note that as noise in our simplified SGD model is Gaussian, such heavy-tailed gradients and superdiffusion dynamics solely result from the fractal loss landscape.

To explicitly illustrate the benefits of fractal landscapes for facilitating the SGD to jump out local minima, we focus on some regions around local minima. As shown in Fig. 8(d), the optimizer moves via step A to this local minimum where the SGD optimizer displays short-range movements as illustrated by step B in Fig. 8(d) and long-range movements as illustrated by step C and D (Fig. 8(d)). Some long-range steps make the SGD optimizer escape the minimum; for example, C goes to a higher altitude and then goes back to the minimum; however, D jumps to a lower altitude and then leaves the minimum. These examples illustrate how the fractal landscape assists the SGD optimizer escape local minima.

As we only use Gaussian noise in this simple model, the main source providing long-range jumps to escape local minima is the heavy-tailed gradients (Fig. 8(c)), supporting the observations in DNNs.

However, if we choose other types of landscapes and maintain  $\eta$  and  $\sigma$ , the complex MSD dynamics no longer hold. When the landscape is generated by smoothing a randomly shuffled fractal landscape such that it is at least once-differentiable, the optimizer gets stuck in a local minimum (Fig. 8(e)) and exhibits subdiffusion (Fig. 8(f)). On the other hand, when the landscape is convex, for example, a convex paraboloid, the MSD has an exponent close to 2 (Fig. 8(f)), inconsistent with the results in DNNs. In comparison to the tail of gradient distribution in fractal landscapes, the ranges of gradients in convex or random landscapes are far smaller (Fig. 8(c)). These results thus indicate the fractal loss landscape is essential for the emergence of the anomalous diffusion learning dynamics.

#### IV. DISCUSSION AND CONCLUSION

We have revealed the anomalous diffusion nature of deep learning dynamics which arises from the interactions of the SGD walker with the geometry structure of the loss landscape. Particularly, we have demonstrated that the fractal-like loss landscape can give rise to the superdiffusion learning dynamics with intermittent big jumps during the initial training phase, which plays an essential role in preventing the SGD optimizer from being trapped in narrow minima. In addition, we have developed a new SGD model to reveal the mechanistic relations between the fractal landscape, the superdiffusive learning dynamics and their computational benefits. Our work sheds light on why deep learning works and suggests certain designing principles for DNNs from a novel perspective.

Previous studies tackled the problem from modeling the SGD as a process with heavy-tailed behaviors [13, 29, 30]. Particularly, Simsekli et al reported a heavy-tailed behavior in the stochastic gradient noise ( $U_t$  in Eq. 2) and proposed modeling the SGD dynamics as a stochastic differential equation driven by an alpha-stable process. They further invoked existing metastability theory to justify why these dynamics would prefer wide minima [13]. The SGD updating rule can be represented in terms of gradient noise, i.e.,  $\mathbf{w}_{k+1} = \mathbf{w}_k - \eta \nabla L(\mathbf{w}_k) - \eta \cdot \text{gradient noise}$ . However, the distribution of gradient noise was further found to be Gaussian in the early phases [31]. Rather than the gradient noise, our work focuses on the drift (i.e., gradient,  $\nabla L(\mathbf{w}_k)$ ) which is directly related to the structure of loss landscape.

The structure of loss landscape can give rise to the anomalous diffusion dynamics of learning process quantified from MSD [16]. Although a previous study [11] also utilized MSD to analyze learning dynamics, it did not introduce/characterize anomalous diffusion in the discus-

sion of learning dynamics. Also, our methods are different from theirs. Baity-Jesi et al. defined MSD by averaging the displacement over all dimensions, like an ensemble-averaged MSD, but does not reflect the same statistical meaning [20], since the dimensions are not independent (anisotropic) [32]. We instead used the time-averaged MSD, which can better demonstrate the anomalous diffusion in the context of DNNs.

By using a similar methodology as in simulated annealing [27], we have quantitatively demonstrated that the loss-landscape of DNN is fractal-like. The fractal-like structure can give rise to heavy-tailed gradients which may help the SGD optimizer to jump out local minima. Also, the fractal landscape may result in fractal trajectories of the SGD optimizer, as in glassy systems [16]. Our results show that the SGD trajectories are indeed fractal as quantified by the contour length and end-to-end length. Recently, it has been suggested that the fractal trajectory of SGD optimizer may facilitate generalization in DNNs [33]. Such fractal trajectories might result from the fractal-like structure of loss landscape as what we have demonstrated.

The simple SGD model does not involve any type of non-Gaussian noise and demonstrates that fractal landscapes alone can lead to anomalous diffusion learning dynamics. However, the emergence of heavy-tailed noise may further facilitate anomalous diffusion dynamics. Anomalous superdiffusion and subdiffusion are nonlinear diffusive processes and are generally referred to as fractional motions that can be formulated based on fractional differential equations [19], suggesting that analyzing such learning dynamics by using fractional formalization would be a promising direction to pursue in the future. Also, future studies should figure out the major source of fractal-like loss landscape. The training landscape is composed of the data and the network architecture. Some previous studies have shown that realistic datasets such as handwritten digits (MNIST), rather than random noise, have low-dimension structure/manifold [34–36]. It would be interesting to study the effect of such data structure on the geometrical properties of loss landscape.

On the other hand, the network structure can affect anomalous diffusion learning dynamics. We find that the deeper DNNs, the shorter scale of superdiffusion, indicating a more demanding training process, consistent with the empirical rules of DNNs [25, 37, 38] and extend the understanding from the aspects of training dynamics and landscape structures [12]. Additionally, shortcut connections in ResNet can extend the scale of superdiffusion, explaining why employing such techniques reduces the difficulties of training DNNs. These findings agree with the theoretical and experimental results of gradient confusion [38] and the visualization of 2D projected loss landscapes [7]. These studies found that shortcut connections enable the training process to become easier. Furthermore, we find that the batch size cannot significantly alter the anomalous diffusion dynamics, supporting the conclusion

that gradient noise is not the only driving force to escape critical points. For future studies, it remains important to find out the quantitative relation of other architectures such as batch normalization [37] and drop out of DNNs and fractal-like landscape structure.

## ACKNOWLEDGMENTS

The authors acknowledge the University of Sydney HPC service for providing high-performance computing

that has contributed to the research results reported within this paper. This work was supported by the Australian Research Council (grant nos. DP160104316, DP160104368).

- 
- [1] Y. LeCun, Y. Bengio, and G. Hinton, *Nature* **521**, 436 (2015).
- [2] Z. C. Lipton, in *The International Conference on Learning Representations (ICLR) workshop* (2016).
- [3] E. Hoffer, I. Hubara, and D. Soudry, in *Advances in Neural Information Processing Systems* (2017) pp. 1731–1741.
- [4] T. J. Sejnowski, *Proceedings of the National Academy of Sciences*, 201907373 (2020).
- [5] A. Choromanska, M. Henaff, M. Mathieu, G. B. Arous, and Y. LeCun, in *Artificial Intelligence and Statistics* (2015) pp. 192–204.
- [6] S. Becker, Y. Zhang, and A. A. Lee, *Physical Review Letters* **124** (2020).
- [7] H. Li, Z. Xu, G. Taylor, C. Studer, and T. Goldstein, in *Advances in Neural Information Processing Systems* (2018) pp. 6389–6399.
- [8] S. Jastrzebski, Z. Kenton, D. Arpit, N. Ballas, A. Fischer, Y. Bengio, and A. Storkey, arXiv:1711.04623 (2017).
- [9] M. Welling and Y. W. Teh, in *Proceedings of the 28th International Conference on Machine Learning* (2011) pp. 681–688.
- [10] P. Chaudhari and S. Soatto, in *Information Theory and Applications (ITA) Workshop* (IEEE, 2018) pp. 1–10.
- [11] M. Baity-Jesi, L. Sagun, M. Geiger, S. Spigler, G. B. Arous, C. Cammarota, Y. Lecun, M. Wyart, and G. Biroli, in *Proceedings of the 35th International Conference on Machine Learning*, Vol. 80 (ACM, 2018) pp. 314–323.
- [12] M. Geiger, S. Spigler, S. d’Ascoli, L. Sagun, M. Baity-Jesi, G. Biroli, and M. Wyart, *Physical Review E* **100**, 12115 (2019).
- [13] U. Simsekli, L. Sagun, and M. Gurbuzbalaban, in *Proceedings of the 36th International Conference on Machine Learning* (2019).
- [14] K. He, X. Zhang, S. Ren, and J. Sun, in *Proceedings of the IEEE conference on computer vision and pattern recognition* (2016) pp. 770–778.
- [15] P. Charbonneau, J. Kurchan, G. Parisi, P. Urbani, and F. Zamponi, *Nature Communications* **5**, 3725 (2014).
- [16] H. J. Hwang, R. A. Riggelman, and J. C. Crocker, *Nature Materials* **15**, 1031 (2016).
- [17] Y. Jin and H. Yoshino, *Nature Communications* **8**, 14935 (2017).
- [18] P. Cao, M. P. Short, and S. Yip, *Proceedings of the National Academy of Sciences*, 201907317 (2019).
- [19] R. Metzler and J. Klafter, *Physics Reports* **339**, 1 (2000).
- [20] V. Zaburdaev, S. Denisov, and J. Klafter, *Reviews of Modern Physics* **87**, 483 (2015).
- [21] T. H. Solomon, E. R. Weeks, and H. L. Swinney, *Physical Review Letters* **71**, 3975 (1993).
- [22] G. M. Viswanathan, S. V. Buldyrev, S. Havlin, M. G. E. Da Luz, E. P. Raposo, and H. E. Stanley, *Nature* **401**, 911 (1999).
- [23] J. Klafter and I. M. Sokolov, *First Steps in Random Walks: from Tools to Applications* (Oxford University Press, 2011).
- [24] S. Hochreiter and J. Schmidhuber, *Neural Computation* **9**, 1 (1997).
- [25] L. Sagun, U. Evci, V. U. Guney, Y. Dauphin, and L. Bottou, in *The International Conference on Learning Representations (ICLR) workshop* (2018).
- [26] M. F. Barnsley, R. L. Devaney, B. B. Mandelbrot, H.-O. Peitgen, D. Saupe, R. F. Voss, Y. Fisher, and M. McGuire, *The Science of Fractal Images* (Springer, 1988).
- [27] G. B. Sorkin, *Algorithmica* **6**, 367 (1991).
- [28] N. Douillet, MATLAB Central File Exchange (2020).
- [29] C. H. Martin and M. W. Mahoney, arXiv:1810.01075 (2019).
- [30] J. Zhang, S. P. Karimireddy, A. Veit, S. Kim, S. J. Reddi, S. Kumar, and S. Sra, arXiv:1912.03194 (2019).
- [31] A. Panigrahi, R. Somani, N. Goyal, and P. Netrapalli, arXiv:1910.09626 (2019).
- [32] Z. Zhu, J. Wu, B. Yu, L. Wu, and J. Ma, in *Proceedings of the 36th International Conference on Machine Learning* (2019).
- [33] U. Şimşekli, O. Sener, G. Deligiannidis, and M. A. Erdogdu, “Hausdorff Dimension, Stochastic Differential Equations, and Generalization in Neural Networks,” (2020).
- [34] J. A. Costa and A. O. Hero, in *European Signal Processing Conference* (2004) pp. 369–372.
- [35] E. Levina and P. J. Bickel, in *Neural Information Processing Systems* (2004) pp. 777–784.
- [36] S. Goldt, M. Mezard, F. Krzakala, and L. Zdeborova, arXiv:1909.11500v3 (2019).
- [37] S. Santurkar, D. Tsipras, A. Ilyas, and A. Madry, in *Advances in Neural Information Processing Systems* (2018) pp. 2483–2493.
- [38] K. A. Sankararaman, S. De, Z. Xu, W. R. Huang, and T. Goldstein, in *Proceedings of the 37th International Conference on Machine Learning* (2020).